Nanoscale

Accepted Manuscript

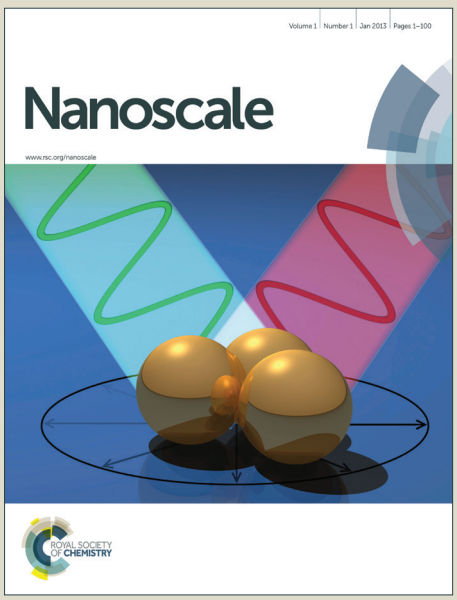

ROYAL SOCIETY OF CHEMISTRY

www.rsc.org/nanoscale

Single-Source-Precursor Synthesis of Dense SiC/HfC_xN_{1-x}-Based Ultrahigh-Temperature Ceramic Nanocomposite

Qingbo Wen[a], Yeping Xu[b], Binbin Xu[c], Claudia Fasel[a], Olivier Guillon[d], Gerd Buntkowsky[b], Zhaoju Yu[e,f,*], Ralf Riedel[a], Emanuel Ionescu[a]

[a] *Technische Universität Darmstadt, Institut für Materialwissenschaft, Jovanka-Bontschits-Straße 2, D-64287, Darmstadt, Germany*

[b] *Technische Universität Darmstadt, Eduard-Zintl-Institut für Anorganische und Physikalische Chemie, Alarich-Weiss-Straße 4, D-64287, Darmstadt, Germany*

[c] *College of Chemistry & Chemical Engineering, Xiamen University, Xiamen 361005, China*

[d] *Otto Schott Institute for Materials Research, Friedrich Schiller University of Jena, Loebdergraben 32, D-07743 Jena, Germany (present address: Forschungszentrum Jülich, Institut für Energie- und Klimaforschung 1: Werkstoffsynthese und Herstellungsverfahren, Wilhelm-Johnen-Straße, D-52425 Jülich)*

[e] *College of Materials, Key Laboratory of High Performance Ceramic Fibers (Xiamen University), Ministry of Education, Xiamen 361005, China*

[f] *College of Materials, Fujian Key Laboratory of Advanced Materials, Xiamen University, Xiamen 361005, China*

Abstract: A novel single-source precursor was synthesized by the reaction of an allyl hydrido polycarbosilane (SMP10) and tetrakis(dimethylamido)hafnium (IV) (TDMAH) for the purpose of preparing dense monolithic SiC/HfC_xN_{1-x}-based ultrahigh temperature ceramic nanocomposites. The materials obtained at the different stages of the synthesis process were characterized via Fourier transform infrared (FT-IR) as well as nuclear magnetic resonance (NMR) spectroscopy. The polymer-to-ceramic transformation was investigated by means of MAS NMR and FT-IR spectroscopy as well as thermogravimetric analysis (TGA) coupled with *in situ* mass spectrometry. Moreover, the microstructural evolution of the synthesized SiHfCN-based ceramics annealed at different temperatures ranging from 1300 ℃ to 1800 ℃ was characterized using elemental analysis, X-ray diffraction, Raman spectroscopy and transmission electron microscopy (TEM). Based on its high temperature behavior, the amorphous SiHfCN-based ceramic powder was used to prepare monolithic SiC/HfC_xN_{1-x}-based

nanocomposites using the spark plasma sintering (SPS) technique. The results showed that dense monolithic SiC/HfC_xN_{1-x}-based nanocomposites with low open porosity (0.74 vol%) can be prepared successfully from single-source precursors. The average grain size of both $HfC_{0.83}N_{0.17}$ and SiC phases was found to be less than 100 nm after SPS processing owing to a unique microstructure: $HfC_{0.83}N_{0.17}$ grains were embedded homogeneously in a β-SiC matrix and encapsulated by *in situ* formed carbon layers which acted as diffusion barrier to suppress grain growth. The segregated Hf-carbonitride grains significantly influenced the electrical conductivity of the SPS processed monolithic samples. While Hf-free polymer-derived SiC showed an electrical conductivity of ca. 1.8 S/cm, the electrical conductivity of the Hf-containing material was analyzed to ca. 136.2 S/cm.

Introduction

HfC, with a melting point of approximately 3900 ℃, is one of the most promising ultrahigh temperature ceramics (UHTCs) due to its high hardness, high elastic modulus, chemical stability, electrical conductivity and relatively high thermal conductivity even under extremely harsh environments.[1,2,3,4] However, the fabrication of dense monolithic HfC ceramic parts is rather challenging, as the self-diffusion in HfC is very low and thus sintering processes of HfC require very high temperatures (usually beyond 2000 ℃), which are disadvantageous concerning grain growth and consequently mechanical properties of the ceramic parts.[5,6,7,8,9,10,11,12] Moreover, HfC and other related UHTC systems (e.g., transition metal carbides, nitrides, borides) suffer from rather poor stability in oxidative environment at high temperatures.[13,14] Thus, composites of UHTCs such as MB_2/SiC and MC/SiC (M = Zr, Hf) have been shown to be more suitable for operation in harsh environments and therefore attracted significant attention in the past decades.[15,16,17]

Recently, nanocomposites received increasing interest because an enormous or even unexpected

improvement in their properties (e.g. mechanical, electrical, optical etc.) can be achieved when reducing the size of the components within the composite materials towards the nano scale.[18,19,20] One of the most suitable preparative routes towards ceramic nanocomposites was shown to rely on the pyrolytic conversion of polymeric single-source precursors.[21,22,23] Thus, the polymer-derived ceramic approach has been a promising method for preparing high temperature ceramic nanocomposites, as the single-source precursors can be tailored at the molecular level in order to design ceramic nanocomposites with unique phase compositions and microstructures and consequently with improved properties.

In the present paper we describe the synthesis of a novel single-source precursor through the reaction of SMP10 with TDMAH, its polymer-to-ceramic transformation as well as the nano/microstructural evolution of the final SiHfCN-based ceramics. Moreover, we present the preparation of dense SiC/HfC_xN_{1-x} ceramic nanocomposites via spark plasma sintering (SPS) of polymer-derived SiHfCN-based ceramic powders and their electrical conductivity behavior.

Experimental Methods

Synthesis of SiHfCN-based ceramics from single source precursor

The single-source precursor for the preparation of the SiHfCN-based ceramics was synthesized using SMP10 (Starfire Systems) and TDMAH (Sigma Aldrich) as starting materials. The synthesis of the single-source precursor was carried out in argon atmosphere (Schlenk Technique) in order to prevent the hydrolysis of the starting materials. Thus, 1.5 g TDMAH was dissolved in 14 mL anhydrous toluene and then added dropwise to a solution of 3.5 g SMP10 in 20 mL anhydrous toluene with stirring at room temperature. The obtained solution was heated at 80 ℃ for 3 h and subsequently the

solvent was removed in vacuum (10^{-2} mbar) at 60 ℃. The as-synthesized single-source precursor was named as Hf-SMP10_80 (i.e., hafnium-modified SMP10, reaction temperature was 80 ℃). The obtained solid Hf-SMP10_80 was ground and pyrolyzed at 1100 ℃ in argon for the preparation of SiHfCN-based ceramic named as SHC-1100. The high temperature behavior of SHC-1100 was investigated upon annealing in argon atmosphere for 5h at 1300 ℃, 1400 ℃, 1500 ℃, 1700 ℃ and 1800 ℃. Monolithic SiC/HfC_xN_{1-x}-based nanocomposite ceramics were prepared from the SHC-1100 powder using Spark Plasma Sintering (SPS) at 2200 ℃ (50MPa, 30min, vacuum). The density and open porosity of the monolithic nanocomposite were measured using the water immersion method.[23]

Characterization

Powder X-ray diffraction (XRD), elemental analysis, Raman spectroscopy and TEM were used to characterize the prepared ceramic materials. Carbon, nitrogen and oxygen contents of ceramics were measured using hot gas extraction techniques through a LECO C-200 and a LECO TC-436 analyzer. Hf and Si content were measured at Mikroanalytisches Labor Pascher (Remagen, Germany). Raman spectra were recorded from 400 cm^{-1} to 4000 cm^{-1} employing a micro-Raman HR8000 spectrometer (Horiba Jobin Yvon, Bensheim, Germany) using a laser wavelength of 514.5 nm.

TGA/MS was carried out with a thermal analysis device (STA 449C Jupiter, Netzsch, Germany) coupled with a quadrupole mass spectrometer (QMS 403C Aëolos, Netzsch, Germany) to study the polymer-to-ceramic transformation of Hf-SMP10_80. The thermal analysis included heating under flowing argon with a rate of 5 ℃/min, holding at 1400 ℃ for 2h and free cooling down to room temperature.

Hf-SMP10_80 was also pyrolyzed at 200 ℃ (Hf-SMP10_200), 400 ℃ (Hf-SMP10_400) and 600 ℃

(Hf-SMP10_600). The obtained materials were studied by solid-state magic-angle spinning nuclear magnetic resonance (MAS NMR) and FT-IR measurements. Moreover, SiHfCN-based ceramics prepared at 800 ℃, 1100 ℃ and 1300 ℃ were also investigated using solid-state MAS NMR.

NMR experiments of the starting materials (SMP10 and TDMAH) were carried out on a Bruker AV 300 NMR spectrometer (Bruker, Germany) operating at 300.13 MHz for ^{1}H, 75.46 MHz for ^{13}C (^{1}H-decoupling) and 59.63 MHz for ^{29}Si (^{1}H-decoupling), and the delay time was 30 s. The solvent for NMR was $CDCl_3$ (for SMP10) and C_6D_6 (for TDMAH). The chemical shifts of ^{1}H, ^{13}C, and ^{29}Si were all referred to tetramethylsilane (TMS) as external standard.

^{13}C and ^{29}Si MAS NMR measurements of Hf-SMP10_80, Hf-SMP10_200, Hf-SMP10_400 and Hf-SMP10_600 were performed on a Bruker AV 300 NMR spectrometer (Bruker, Germany) using a 4.0 mm Bruker double resonance MAS probe with a spinning speed of 5.0 kHz. The ^{13}C isotropic chemical shifts were referenced to the carbonyl carbon of glycine (assigned to 173.2 ppm). In addition, ^{29}Si and ^{13}C MAS NMR spectra of SiHfCN-based ceramics prepared at 800 ℃, 1100 ℃ and 1300 ℃ were measured using the single pulse (SP) technique operating at 125.79MHz for ^{13}C and at 99.38MHz for ^{29}Si. Both ^{13}C and ^{29}Si MAS NMR spectra were recorded using a 90 °pulse of 6 μs and recycle delays of 60s. ^{29}Si and ^{13}C chemical shifts were determined relative to the external standards kaolin and adamantane, respectively, and are given with respect to the primary standard TMS (δ = 0 ppm).

Transmission electron microscopy (TEM) studies were conducted on ground powder samples using a JEM-2100 (Japan) microscope at an acceleration voltage of 200 kV (wavelength l52.51 pm) coupled with an electron diffraction spectroscope (EDS, EDAX, USA). In addition, the selected area electron diffraction (SAED) technique was employed in order to investigate the phase separation and nucleation of the Hf containing phase.

The electrical conductivity of the as-prepared monolithic SiC/HfC_xN_{1-x}-based nanocomposite was measured using the four-point probe method with square arrangement probes. Thus, a KEITHLEY 224 was used as a programmable current source and a KEITHLEY 2010 multimeter was used for voltage measurement. The four-point probes were placed in the center of the monolithic samples which were polished with 1μm SiC on felt cloth. The electrical conductivity of dense monolithic Hf-free SiC-based ceramics obtained by SPS of pure SMP10-derived ceramic powders was also measured for the sake of comparison.

Results and Discussion

Synthesis of the single-source precursor

As mentioned above, the single source precursor, i.e. Hf-SMP10_80, was synthesized by the reaction of SMP10 with TDMAH. During the synthesis, samples were collected at different steps for FT-IR spectroscopy measurement and the spectra of the precursors reacted at room temperature (RT) and at 80 ℃ are shown in Figure 1a. The spectra of pure SMP10 at room temperature as well as heated at 80 ℃ for 3 h are also shown in Figure 1 for comparison. Upon TDMAH addition to pure SMP10 at room temperature, the absorption bands assigned to the allyl groups (C-H stretching at 3075cm^{-1} and C=C stretching at 1630 cm^{-1})[24] disappear and the relative intensity of the Si-H band (Si-H stretching at 2115cm^{-1}) significantly decreases with respect to the intensity of the Si-CH_3 band (Si-C stretching at 747cm^{-1}),[25] while new bands due to Hf-NCH_3 groups appear, including C-H stretching at 2788 $cm^{-1}$and N-CH_3 bending 1450 cm^{-1} as well as the characteristic vibrations of Hf-N-C units at 945 cm^{-1}.[26] After heating at 80 ℃ for 3 h, the relative intensity of the Si-H band at 2115cm^{-1} in the spectrum labeled (4) decreases further, while those of the Hf-NCH_3 bands change slightly.

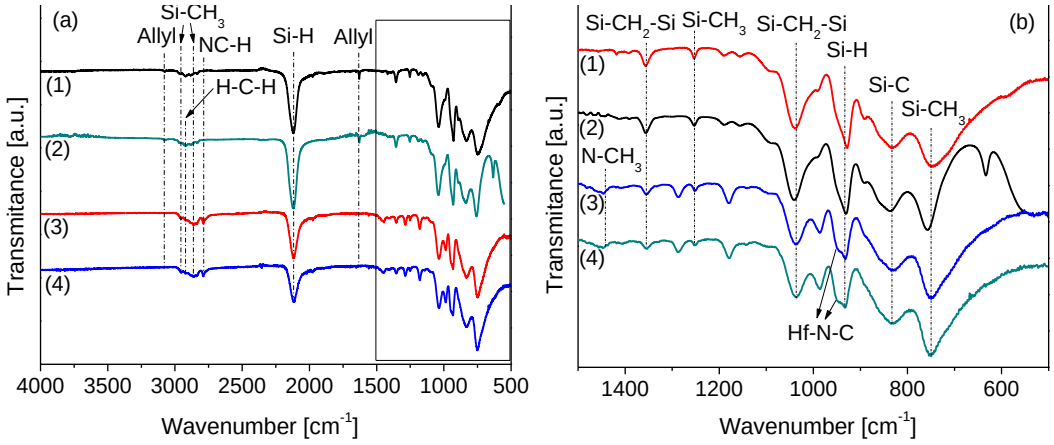

Figure1. FT-IR spectra of precursors before and after reaction are shown in (a), and the region from 500 to 1500 cm^{-1} is shown magnified in (b): (1) SMP10_RT, (2) SMP10_80, (3) Hf-SMP10_RT, (4) Hf-SMP10_80; RT = room temperature.

According to previous reports,[27,28] two reaction pathways occur during the synthesis of Hf-SMP10_80 (Figure 2). The first one involves the hydrosilylation of the allyl groups, which explains the disappearance of allyl groups and the decrease in the intensity of Si-H peaks. As the hydrosilylation process starts at temperatures of ca. 100-120 ℃,[21] the pure SMP10 heated at 80 ℃ (spectrum (2) in Figure 1a) did not show significant changes of the intensities of the allyl and Si-H vibrations. However, the addition of TDMAH to SMP10 induces the disappearance of the absorption bands of the allyl groups even at room temperature (spectrum (3) in Figure 1a), which indicates that the TDMAH acts as a catalyst for the hydrosilylation.[29,30] The second reaction route involves the reaction of TDMAH with the Si-H groups of SMP10, which leads to the formation of Si-N-Hf linkages. Li et al. calculated bond dissociation energies using density functional theory and they roughly follow the order of Hf-N > C-H/Si-N > Si-H/Si-C > N-C/Hf-H > Hf-Si.[26] This information was corroborated with chemisorption experiments of TDMAH on Si substrates to suggest that the reaction between TDMAH and hydrogen terminated Si (100) surfaces occurs through the formation of Si-N bonds, which is more probable than that of Si-Hf bonds.

Based on the two reaction pathways, synthesis of the single-source precursor from SMP10 and TDMAH can be describes as depicted in Figure 2: the allyl and Si-H groups of SMP10 are involved in hydrosilylation which leads to an increased cross-linking degree of the precursor; additionally, TDMAH reacts with the Si-H groups of SMP10 to form Si-N-Hf linkages and gaseous CH_4.

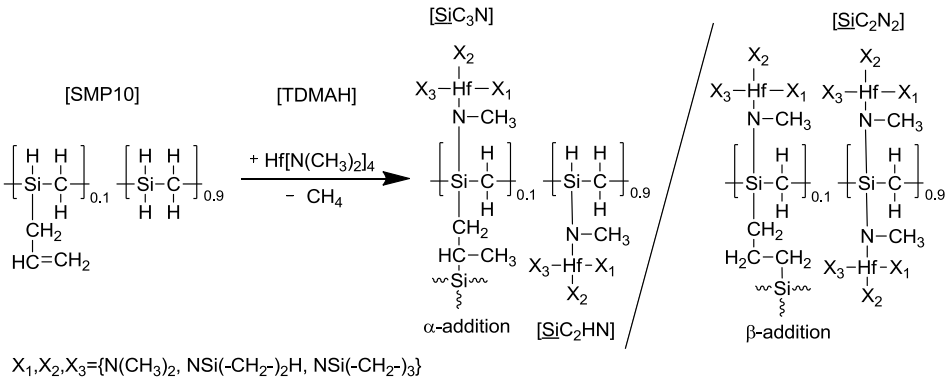

Figure 2. Reaction pathways during synthesis of the single-source precursor from SMP10 and TDMAH.

According to the ^{29}Si NMR spectra, there are three kinds of hydrogen-bearing Si sites (hydrido silyl groups), as alternating groups of the polymer backbone of SMP10, i.e. C<u>Si</u>H_3, C_2<u>Si</u>H_2 and C_3<u>Si</u>H.[31] Hence, different kinds of <u>Si</u>-N(CH_3)-Hf units including C<u>Si</u>H_2N, C<u>Si</u>HN_2, C<u>Si</u>N_3, <u>Si</u>C_2HN, <u>Si</u>C_2N_2 and <u>Si</u>C_3N can be generated upon reacting the corresponding Si-H groups with TDMAH. In order to further investigate the reaction between SMP10 and TDMAH in more detail and to confirm the molecular structure of the obtained precursor, ^{13}C and ^{29}Si NMR analysis was conducted on the pure SMP10, TDMAH, as well as on Hf-SMP10_80 and the results are shown in Figure 3.

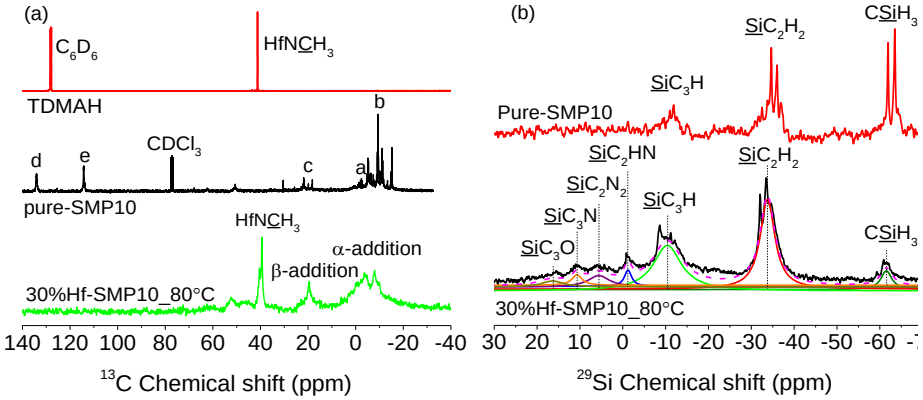

Figure 3. NMR spectra of starting materials (TDMAH and SMP10) and MAS NMR spectra of Hf-SMP10_80: (a) ^{13}C and (b) ^{29}Si spectra.

In the ^{13}C NMR spectrum of SMP10 (Figure 3a), the chemical shifts of 134.3 ppm and 114.7 ppm are assigned to the carbon sites of ≡Si–CH_2–$\underline{C}H$=CH_2 (d) and ≡Si–CH_2–CH=$\underline{C}H_2$ (e) of the allyl groups, respectively. Multiple chemical shifts in the region from 17.7 to 30.0 ppm are attributed to the ≡Si–$\underline{C}H_2$–CH=CH_2 (c) linkage between silicon and the allyl groups. The signal of the ≡Si-$\underline{C}H_3$ groups was observed around 2.4 ppm and the chemical shifts from -4.4 to -16.0 ppm were assigned to ≡Si–$\underline{C}H_2$–Si linkages on the main chain (b).[24] Compared with the ^{13}C spectrum of pure SMP10, the allyl-carbon resonances (d and e) of the Hf-SMP10_80 disappeared due to the hydrosilylation process, which is consistent with the FT-IR results. A new broad resonance appeared in the region from 16 to 21 ppm, which was assigned to the carbon sites of ≡Si-CH_2-$\underline{C}H_2$-CH_2-Si≡ units derived from the β-addition product, while the resonance assigned to the methylene carbon of the ≡Si-CH_2-$\underline{C}H(CH_3)$-Si≡ $SiCH_2\underline{C}H(CH_3)Si$ units derived from the α-addition product was overlapped with those of the ≡Si-$\underline{C}H_3$ (a) units and ≡Si-$\underline{C}H_2$-Si≡ (b) groups from SMP10.[31] Concerning the hydrosilylation, the NMR results agree well with the reaction paths shown in Figure 2. The spectrum of Hf-SMP10_80 shows one broad additional resonance around 41 ppm, which was assigned to =N-$\underline{C}H_3$ groups stemming from the Hf-N$\underline{C}H_3$ units of the precursor, thus supporting the reaction between SMP 10 and TDMAH.

The ^{29}Si NMR signals of pure SMP10 were already published and are shown in Figure 3b according to the references.[24,32] If compared with pure SMP10, the integral of the peaks in the spectrum of Hf-SMP10_80 clearly show that the contents of C*Si*H$_3$ and *Si*C$_2$H$_2$ units are decreased, indicating that both the hydrosilylation of SMP10 and the reaction between SMP10 and TDMAH occur. As aforementioned, new silicon units including C*Si*H$_2$N, C*Si*HN$_2$, C*Si*N$_3$, *Si*C$_2$HN, *Si*C$_2$N$_2$ and *Si*C$_3$N are supposed to form in the obtained Hf-SMP10_80 precursor. However, in the ^{29}Si MAS NMR spectrum of Hf-SMP10_80, only three new signals were analyzed and assigned to *Si*C$_3$N, *Si*C$_2$N$_2$ and *Si*C$_2$HN units, exhibiting site fractions of 1.9 , 2.1 and 4.4 %, respectively (Table 1).[33]

In conclusion, the NMR results clearly indicate that the reaction between TDMAH and SMP10 resulted in the formation of a single-source precursor (i.e., Hf-SMP10_80), which was subsequently investigated concerning its polymer-to-ceramic transformation.

Polymer-to-ceramic transformation

The structural evolution during the polymer-to-ceramic conversion of the single-source precursor Hf-SMP10_80 was studied by a combination of FT-IR (Figure 4), ^{13}C and ^{29}Si MAS NMR (Figure 5) and *in situ* TGA/MS (Figures 6 and 7) studies. As shown in Figure 4a, the intensities of the Si-H and N-CH$_3$ vibrations have only slight changes with the temperature increasing from 80 ℃ to 200 ℃. However, the intensity of the N-CH$_3$ absorptions decreases significantly after pyrolysis at 400 ℃ due to the further reaction between the N-CH$_3$ groups of TDMAH and the Si-H groups of SMP10 (NCH$_3$/Si-H). The bands of the Si-H vibration at 2115 cm^{-1} and 930 cm^{-1} also decrease due to dehydrocoupling (Si-H/Si-H) and further reactions between TDMAH and SMP10 (NCH$_3$/Si-H).

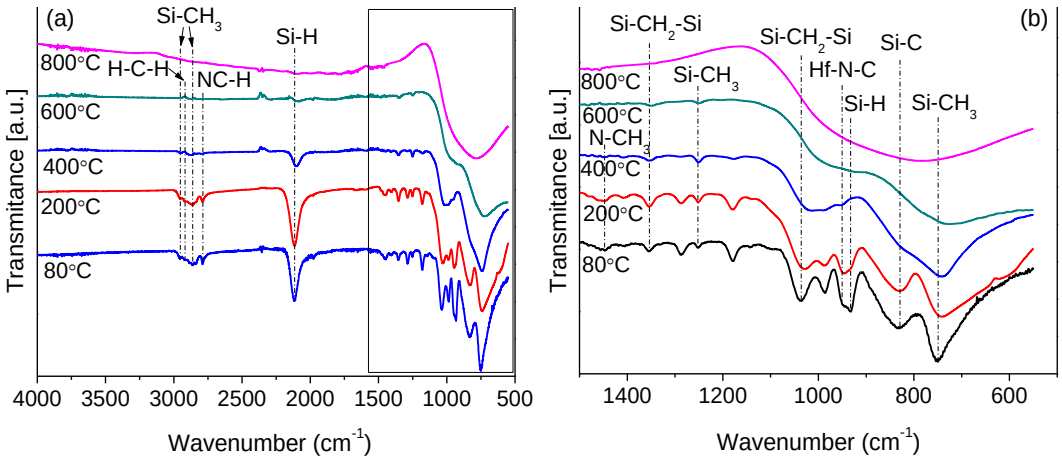

Figure 4. (a) FT-IR spectra of Hf-SMP10_80 heat-treated at different temperatures; (b) magnification of the region from 500 to 1500 cm^{-1}.

At temperature beyond 600 ℃, the peaks for the NC-H stretching vibration at 2788 cm^{-1} and N-CH_3 bending at 1450 cm^{-1} disappear while the characteristic absorption band of Hf-N-C at around 945cm^{-1} still exists, overlapping with broad Si-C peaks (Figure 4b). The intensities of the Si-CH_3 absorption bands at 2955, 2861 and 1250 cm^{-1} as well as that of the Si-CH_2-Si bands at 2920, 1035 and 1353 cm^{-1} decrease, which is attributed to the decomposition of the organic groups.

^{13}C and ^{29}Si MAS NMR analysis was also performed and the results are shown in Figure 5 and Table 1. As shown in Figure 5a, the intensity of the carbon signal of the Hf$N\underline{C}H_3$ units significantly reduces with the temperature increasing from 200 ℃ to 400 ℃ and disappears at 600 ℃, indicating that the amido groups are consumed by the reaction between TDMAH and SMP 10 (NCH_3/Si-H), which is consistent with the FT-IR results.

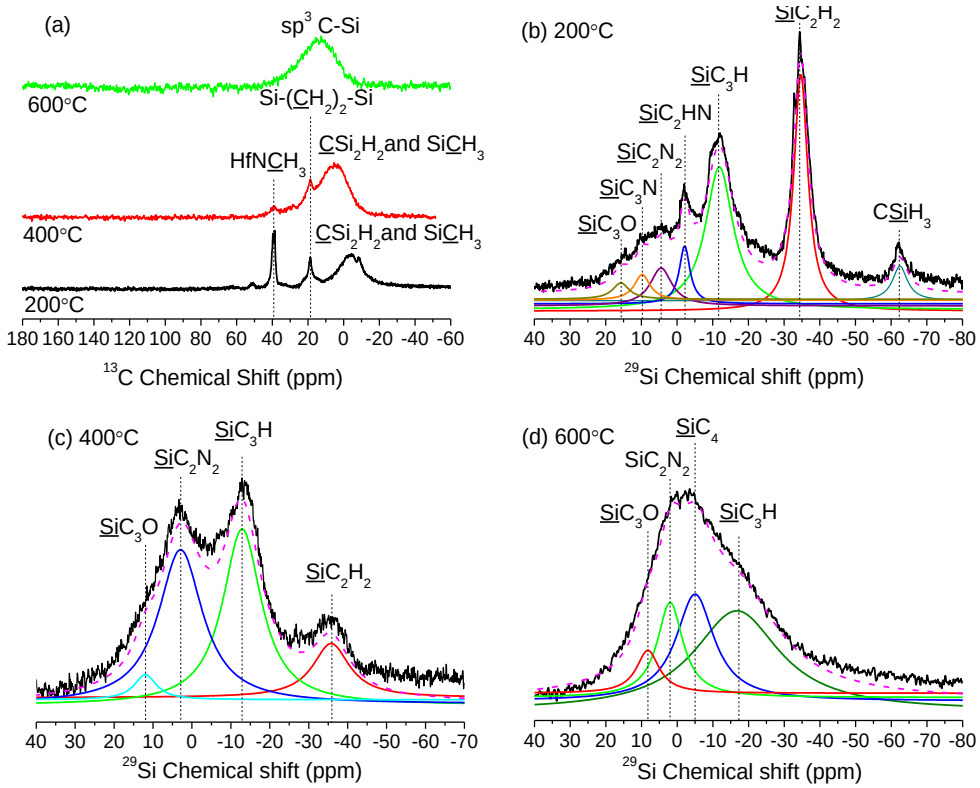

Figure 5. ^{13}C and ^{29}Si MAS NMR spectra of Hf-SMP10_200, Hf-SMP10_400 and Hf-SMP10_600. (a): ^{13}C spectra; (b), (c) and (d): ^{29}Si MAS NMR spectra. The black solid bold lines are the experimental spectra, the dashed lines represent the simulated spectra and the colorful solid lines indicate the individually fitted components.

From 80°C to 200 °C, the chemical shifts of the ^{29}Si signals changed slightly and the fractions of $\underline{Si}C_3N$, $\underline{Si}C_2HN$ and $\underline{Si}C_2N_2$ units increase owing to the progress of the reaction between TDMAH and SMP10 (NCH_3/Si-H) (Table 1). With the temperature increasing from 200 °C to 400 °C, the $C\underline{Si}H_3$ units almost disappear and the intensity of the $\underline{Si}C_2H_2$ signal decreases considerably while those of the $\underline{Si}C_3H$ signals increase (Table 1, Figures 5b and 5c), due to Si-H/Si-H dehydrocoupling reactions.[34] The signals of $\underline{Si}C_2HN$ and $\underline{Si}C_3N$ units disappear and that of $\underline{Si}C_2N_2$ becomes stronger and broader with a fraction up to 42.2 %, indicating a significant reaction between N-CH_3 and Si-H groups ($NCH_3/\underline{Si}C_2H_2$ and $NCH_3/\underline{Si}C_2HN$) upon generating additional $\underline{Si}C_2N_2$ units. Subsequently, after pyrolysis at 600°C, the signal related to $\underline{Si}C_2H_2$ units disappear and a new peak assigned to $\underline{Si}C_4$ units (-5 ppm) appear due to Si-H/Si-H dehydrocoupling (Figure 5d).[31]

The NMR and FT-IR spectroscopic results were further supported by the results of the *in situ* TG/MS analysis. As shown in Figure 6, the TG and DTG curves (first time derivative of the TG) revealed that there are 3 main steps during the pyrolysis of Hf-SMP10_80.

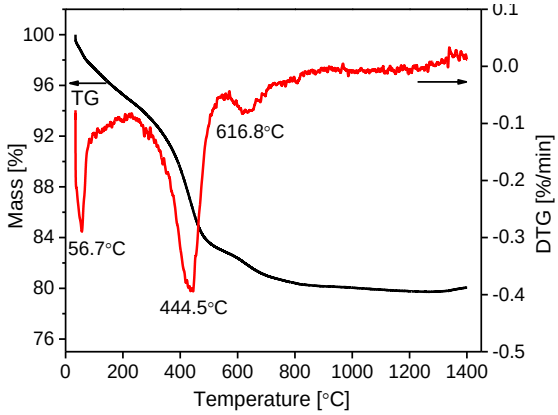

Figure 6. TG and DTG (first derivative of the TG) curves of ceramization process of Hf-SMP10_80.

The first step started from ambient temperature to approximately 200 ℃ with the DTG peak at 56.7 ℃. During this step, a small weight loss was observed and slight release of CH_4 (Figure 7a, *m/z* = 15) was detected, which relies on the reaction between TDMAH and SMP 10 (N-CH_3/Si-H), leading to the decomposition of N-CH_3 groups. However, the decomposition of the N-CH_3 groups was not significant at these temperatures, as the intensity of N-$\underline{C}H_3$ in the ^{13}C MAS NMR spectrum of Hf-SMP10_80 pyrolyzed at 200 ℃ (Figure 5a) is still very high. This behavior is different from that of the pure TDMAH, which fully decomposes at temperatures beyond 150 ℃.[26]

In the temperature range from 200 to 600 ℃, two evolution peaks of CH_4 were detected. At 490 ℃, the first release of CH_4 was observed, leading to the weight loss during ceramization process. The CH_4 is generated from the further reaction between TDMAH and SMP10 (reaction between NCH_3 and Si-H groups), which was substantiated by FT-IR and solid-state MAS NMR results. Moreover, the release of amines was also detected during the temperature range from 250 to 600 ℃ (Figures 7b and 7c) and ammonia was detected at temperatures from 340 to 780 ℃ (Figure 7a) as well, suggesting that

transamination occurred during the ceramization process. This was further supported by *ex situ* FTIR and MAS NMR investigations on the samples pyrolyzed at 200, 400 and 600 ℃. Furthermore, some fragments derived from hydrocarbons such as C_2H_6 (from 300 to 680 ℃, Figure 7b), C_3H_8 (from 250 to 620 ℃, Figure 7c) and C_4H_{10} (from 250 to 620 ℃, Figure 7d) were detected as well; their release relies on the decomposition of the organic substituents in the single-source precursor decomposition. The ceramization process was found to be completed at approximately 900 ℃ (i.e., beyond this temperature no mass loss was observed), leading to a ceramic yield of *ca*. 80 wt%.

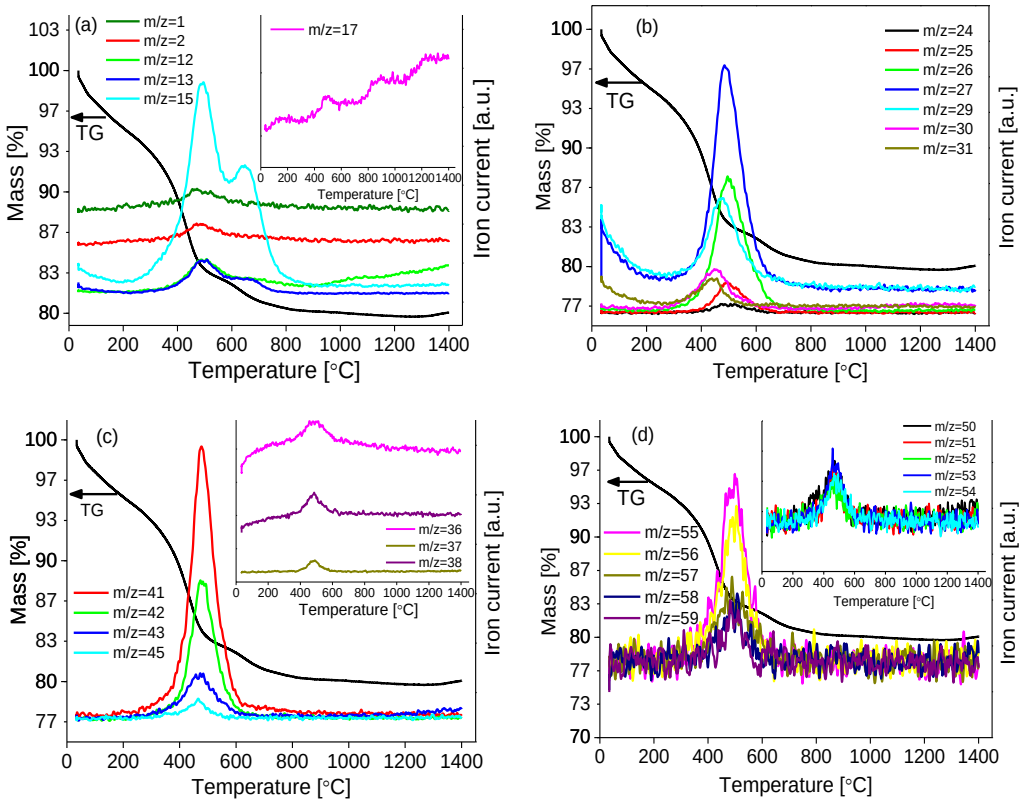

Figure 7. TG and QMID ion current curves (QMID - quasi multiple ion detection) describing the evolution of volatile species during the polymer-to-ceramic transformation of Hf-SMP10_80 (a: hydrogen (*m/z* = 1 and 2), methane (*m/z* = 12, 13 and 15) and ammonia (*m/z* = 17); b: amines and C_2H_6 (*m/z* = 24, 25, 26, 27, 29, 30 and 31); c: amines and C_3H_8 (*m/z* =36, 37, 38,41, 42, 43 and 45); d: C_4H_{10}.

Table 1. ^{29}Si MAS NMR chemical shifts and fractions of the silicon containing units in the precursors and pyrolytic residues at different temperatures.

Temperature	$\underline{Si}C_3N$		$\underline{Si}C_2HN$		$\underline{Si}CH_3$		$\underline{Si}C_2H_2$	
[℃]	[ppm]	[%]	[ppm]	[%]	[ppm]	[%]	[ppm]	[%]
80	10.69	3.1	-1.22	3.4	-61.53	6.0	-33.78	38.8
200	9.78	4.1	-2.12	6.2	-62.47	5.2	-34.80	33.6
400	---	---	---	---	---	---	-35.75	12.2
Temperature	$\underline{Si}C_2N_2$		$\underline{Si}C_3H$		$\underline{Si}C_4$		$\underline{Si}C_3O$	
[℃]	[ppm]	[%]	[ppm]	[%]	[ppm]	[%]	[ppm]	[%]
80	5.59	7.2	-10.41	37.6	---	---	16.40	3.9
200	4.49	8.2	-11.86	40.1	---	---	15.76	2.7
400	2.93	42.2	-12.89	42.1	---	---	11.97	3.4
600	1.99	15.2	-16.70	53.6	-5.00	25.2	8.23	6.1
800	-5.73	19.0	---	---	-13.43	76.7	7.39	4.3
1100	-10.87	19.2	---	---	-16.56	79.1	3.97	1.7
1300	-22.60	2.3	---	---	-17.27	93.5	0.20	4.1

Microstructural evolution of the as-prepared ceramics

After pyrolysis of Hf-SMP10_80 at 1100 ℃ in argon atmosphere, a black ceramic was obtained (i.e., SCH-1100). The synthesized ceramic was subsequently annealed in argon atmosphere at 1300, 1400, 1500, 1700 and 1800 ℃ in order to investigate its high temperature behavior with respect to decomposition, phase separation as well as crystallization. After annealing at different temperatures, the relative weight loss with respect to the sample SHC-1100 and the elemental contents of Hf, Si, C, N and O in the obtained ceramic materials were analyzed and the results are listed in Table 2. Considering that the SiC yield of pure SMP10 amounts 72-78 wt%, the weight ratio of TDMAH:SMP10 is 30:70, and assuming that Hf segregates as HfC in the obtained ceramics, the HfC content can be estimated to be 23-24 wt% and agrees well with the experimentally determined HfC contents (e.g., 24 wt% HfC in SHC-1700). Consequently, the loss of Hf during polymer-to-ceramic transformation of the single-source precursor and during the high-temperature annealing of the ceramic materials is considered to be negligible.

Table 2. Weight loss and chemical composition of ceramics annealed at different temperatures.

Sample	Processing temperature	Mass loss (wt%)*	Elemental analysis (wt%)					Empirical formula
			Si	Hf	C	N	O	
SHC-1100	1100 ℃	-	45.80	20.00	25.14	3.86	3.89	$SiHf_{0.07}C_{1.28}N_{0.17}O_{0.15}$
SHC-1300	1300 ℃	0.92%	*n.d.*	*n.d.*	25.26	3.78	3.66	*n.d.*
SHC-1400	1400 ℃	2.31%	*n.d.*	*n.d.*	24.98	3.96	3.49	*n.d.*
SHC-1500	1500 ℃	11.1%	*n.d.*	*n.d.*	25.80	1.97	1.52	*n.d.*
SHC-1700	1700 ℃	14.23%	51.00	22.90	24.94	0.28	0.14	SiC 0.06HfC 0.01HfN 0.071C
SHC-1800	1800 ℃	14.76%	*n.d.*	*n.d.*	24.89	0.13	0.08	*n.d.*

* - weight loss with respect to the as-prepared ceramic (i.e., SHC-1100); n.d.: not determined

As shown in Table 2, the weight loss of the ceramics annealed at temperatures below 1400 ℃ is low and the contents of C, N and O are only slightly changed. A relatively obvious weight loss occurred at 1500 ℃ due to the loss of N and O.[35] After the release of N and O, the weight loss increased marginally, even upon annealing for 5 h at 1800 ℃. This result suggests a promising high temperature stability of the synthesized SiHfCN-based ceramics.

In order to investigate the temperature evolution of the prepared SiHfCN-based ceramics, ^{29}Si and ^{13}C MAS NMR spectra of the ceramics prepared at 800 ℃, 1100 ℃ and 1300 ℃ were measured and deconvoluted using Lorentz fitting. As shown in Figure 8, there is a broad ^{29}Si resonance in the spectra of the ceramics pyrolyzed at 800, 1100, and 1300 ℃, indicating the heterogeneous amorphous nature of the local environment around the Si atoms.[31,36]

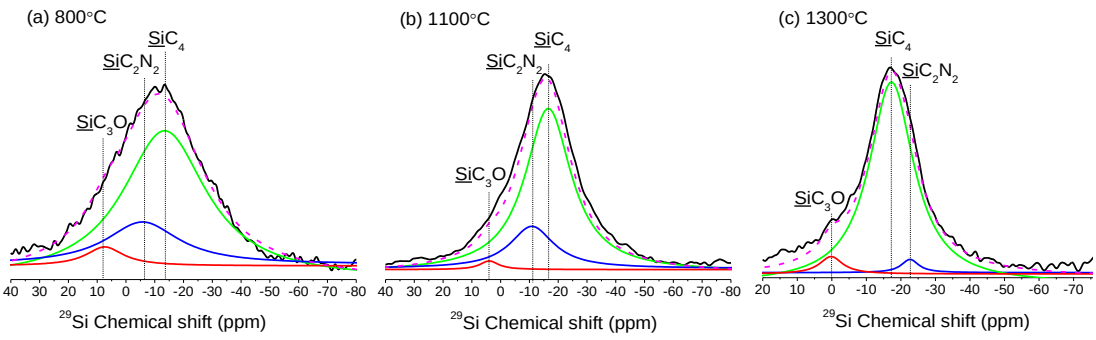

Figure 8. ^{29}Si MAS NMR spectra of SiHfCN-based ceramics pyrolyzed at 800 ℃ (a), 1100 ℃ (b) as well as annealed at 1300 ℃ (c).

As aforementioned, the Hf atoms are connected of SMP10 by Hf-N(CH_3)-Si units to the polymeric backbone of the single-source precursor (Figure 2). During the pyrolysis process, part of the nitrogen atoms at the Hf sites might be substituted by C atoms due to transamination processes.[26] Thus, in the ceramic pyrolyzed at 800 ℃ Hf atoms might be connected to the amorphous matrix by Hf-N and Hf-C bonds. This assumption is supported by the low-field shift of the ^{29}Si resonances of the $\underline{Si}C_2N_2$ and $\underline{Si}C_4$ sites (Figures 5 and 8). It is known from literature that in SiCN samples obtained at 600 ℃, the chemical shift $\underline{Si}C_2N_2$ sites is ca. -7.5 ppm,[34] while in our Hf-containing sample they exhibit a significant low-field shift to ca. 1.99 ppm. This is considered to rely on the presence of Hf in the proximity of SiC_2N_2 sites, which is responsible for the decrease of the electronic density at Si. Analogous trends were also found in SiMOC materials (M = Zr [37], Hf [23]), in which the ^{29}Si chemical shifts SiO_4 sites were significantly low-field shifted due to the presence of Zr/Hf bonded to the SiO_4 tetrahedra. Also the $\underline{Si}C_2N_2$ and $\underline{Si}C_4$ sites (with chemical shifts of ca.-12 and -15 ppm, respectively)[34] are shifted to low field (i.e., -5.73 and -13.43 ppm, respectively), due to the existence of Si-N-Hf and Si-C-Hf linkages.

As the heat treatment temperatures increases (e.g., to 1100 ℃), HfC_xN_{1-x} starts to segregates (i.e., phase separation of SiHfCN upon breaking of Si-N-Hf and Si-C-Hf linkages), which consequently leads to a high-field shift of the ^{29}Si resonances of the $\underline{Si}C_2N_2$ and $\underline{Si}C_4$ sites (Table 1). The phase separation is not significant at 1100 ℃, thus the $\underline{Si}C_2N_2$ sites are still significantly low-field shifted (-10.9 ppm) as compared to $\underline{Si}C_2N_2$ sites in Hf-free SiCN (-17 ppm) (see Table 1). Whereas after annealing at 1300 ℃ both $\underline{Si}C_2N_2$ (-22.6 ppm) and $\underline{Si}C_4$ sites (-17.3 ppm) show similar chemical shifts to those of Hf-free SiCN materials (Table 1).[38] The presence of small amounts of $\underline{Si}C_3O$ units (< 6%) in the investigated samples (Table 1, Figures 5 and 8) has been explained as a consequence of some

oxygen contamination during the processing of the single-source precursor.[23, 39]

The ^{13}C MAS NMR spectra in Figure 9 show that the resonances for the carbon sites of the C-N-Hf units (chemical shift at 37.9 ppm) exist in the samples prepared at 800, 1100, and 1300 ℃ even after the phase separation of SiHfCN, suggesting that some Hf is still present within the ceramic matrix after the segregation of HfC_xN_{1-x}. This has been reported also in SiHfOC ceramics, where the presence of Hf within SiOC matrix after the segregation of HfO_2 was found to be responsible for the coarsening of the HfO_2 precipitations upon high-temperature annealing of the nanocomposites.[40, 41] Additionally, the presence of segregated sp^2 carbon in the investigated materials is obvious. In Figure 9a, the ^{13}C resonance at 138.07 ppm was assigned to sp^2 C-C with one or more Si nearest neighbors,[42] indicating that the segregated carbon phase is connected to the SiHfCN matrix via C-Si bonds after pyrolysis at 800 ℃. In the materials heat-treated at higher temperatures, two types of sp^2 carbon sites were found (Figure 9b), namely one with a chemical shift of 164.10 ppm, which was assigned to nitrogen-containing sp^2 carbon and a second resonance located at 127.49 ppm which corresponds to turbostratic carbon (sp^2 C-C). [42,43]

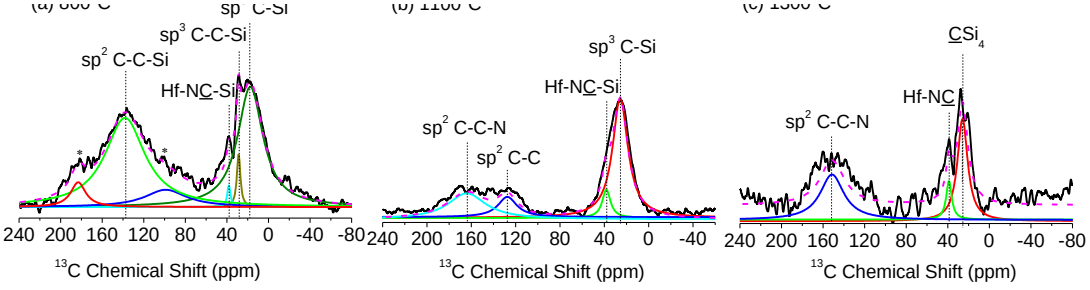

Figure 9. ^{13}C MAS NMR spectra of ceramics prepared at 800 ℃, 1100 ℃ and annealed at 1300 ℃ (the peaks denoted with asterisks are the spinning side bands).

After annealing at 1300 ℃ (Figure 9c), the peak corresponding to the nitrogen-containing sp^2 carbon was found to be shifted to high field (chemical shift at 151.44 ppm). Hence, from the NMR data it can be concluded that the ceramics pyrolyzed at 800 ℃ are mainly comprised of an amorphous SiHfCN

single phase connected to carbon-rich domains, and that the phase separation of HfC_xN_{1-x} starts after pyrolysis at 1100 ℃ and is almost completed after annealing at 1300 ℃.

In order to investigate the crystallization behavior of the SiHfCN-based ceramics, X-ray diffraction patterns (XRD) of the ceramic materials annealed at different temperatures were measured and the results are shown in Figure 10.

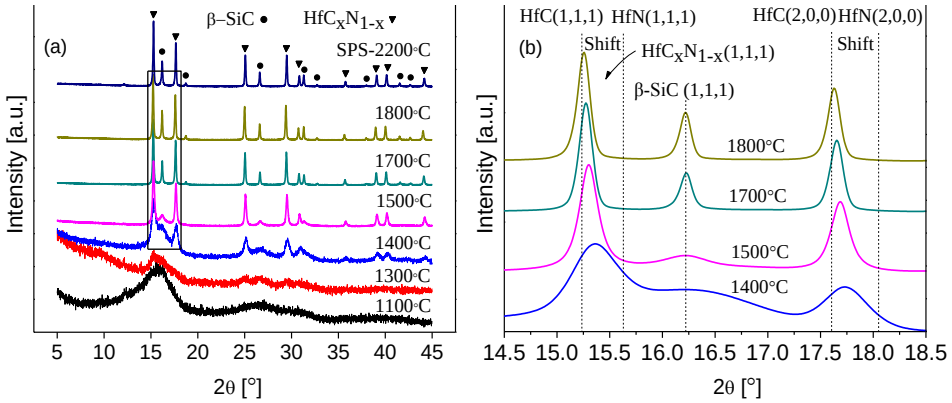

Figure 10. (a) XRD patterns of the ceramics pyrolyzed and annealed at different temperatures as well as sintered at 2200 ℃. (b) the region in the rectangle is shown magnified.

The XRD patterns reveal that the ceramic prepared at 1100 ℃ is mainly X-ray amorphous, while with increasing annealing temperatures, crystallization of both HfC_xN_{1-x} and β-SiC takes places. Interestingly, the Hf-containing phase was found to contain some amount of nitrogen (i.e., HfC_xN_{1-x}). According to Hume-Rothery rules, cubic HfC and HfN are able to form complete quasi-binary solid solutions, as both of them are interstitial compound having fcc structure and the covalent radii of the C and N atoms differ by only 2.60 %.[44,45] The volume fractions, grain sizes and lattice constants of HfC_xN_{1-x} and β-SiC obtained by Full-Profile Rietveld refinement of the XRD patterns of the investigated samples, are listed in Table 3.

Table 3. Volume fractions, grain sizes and lattice constants of HfC_xN_{1-x} and β-SiC as well as the estimated compositions of HfC_xN_{1-x} in the ceramics annealed at different temperatures.

Sample	Volume fraction (%)		Estimated grain size (nm)		Lattice Constant, *a* (Å)		Estimated Composition of HfC_xN_{1-x}
	HfC_xN_{1-x}	SiC	HfC_xN_{1-x}	SiC	HfC_xN_{1-x}	SiC	
SiHC-1400	1.71	98.29	5.61	1.63	4.6020	4.3445	$HfC_{0.68}N_{0.32}$
SiHC-1500	6.99	93.01	18.12	3.59	4.6132	4.3469	$HfC_{0.78}N_{0.22}$
SiHC-1700	11.01	88.99	45.11	33.41	4.6231	4.3519	$HfC_{0.87}N_{0.13}$
SiHC-1800	10.11	89.89	51.59	54.59	4.6309	4.3561	$HfC_{0.93}N_{0.07}$
SPS-2200 ℃	8.58	91.41	80.87	36.63	4.6184	4.3563	$HfC_{0.83}N_{0.17}$

As shown in Figure 10b, the reflections of the HfC_xN_{1-x} phase shift towards low 2θ values upon increasing the annealing temperature, i.e., the HfC_xN_{1-x} phase becomes enriched in carbon. As previously reported, the lattice constant of HfC_xN_{1-x} is a linear function of its chemical composition which obeys Vegard's law.[45, 46] Thus, the observed shift of the XRD reflections in Figure 10b (as for the (111) and (200) reflections) was used to estimate the chemical composition of the HfC_xN_{1-x} phase in the ceramics prepared at different temperatures (Table 3).[47]

The composition of the HfC_xN_{1-x} phase can be estimated also from the chemical composition of the samples. For the sample SiHC-1700 (with the chemical composition $SiC_{1.14}Hf_{0.07}N_{0.01}(O_{0.005})$), the composition of the HfC_xN_{1-x} phase is $HfC_{0.86}N_{0.14}$ and agrees very well with the composition estimated by the Vegard's law from the XRD pattern ($HfC_{0.87}N_{0.13}$, Table 3).

The synthesized SiHfCN-based ceramics annealed at different temperatures ranging from 1100 to 1700 ℃ were further studied by means of TEM in order to assess the evolution of their phase composition and microstructure at high temperatures (Figures 11 and 12). In Figure 11a, the ceramic prepared at 1100 ℃ is amorphous, as revealed by the featureless selected area electron diffraction (SAED) pattern. However, contrast variations indicate that the phase segregation of HfC_xN_{1-x} occurred, as shown in the high-resolution micrograph in Figure 11b, which shows small nuclei of HfC_xN_{1-x} with

diameter less than 2 nm dispersed homogeneously throughout the matrix. After annealing at 1300 ℃, HfC_xN_{1-x} precipitations (dark contrast) with an average particle size of ca. 2.5 nm were found to be homogeneously dispersed within a silicon carbide matrix (Figures 11c and 11d). In the high-resolution micrograph lattice fringes of the poorly crystallized HfC_xN_{1-x} nanoparticles can be observed. Although no β-SiC crystallites were visualized, the SAED pattern clearly indicates the crystallization of β-SiC and thus agrees with the XRD results.

The TEM micrographs of the ceramics annealed at 1400 and 1700 ℃ are shown in Figure 12 and show the presence of HfC_xN_{1-x} embedded within a β-SiC matrix, as shown also by EDS analysis. After annealing at 1700 ℃, β-SiC crystallites can be identified (see Figure 12d). Interestingly, the size of the SiC nanoparticles (few nanometers) was significantly lower than that estimated by Rietveld refinement (ca 33 nm, see Table 3).

The sample annealed at 1400 ℃ is characterized by a unique microstructure. As depicted in Figure 12, the HfC_xN_{1-x} nanoparticles are encapsulated within a layer of carbon (thickness ca. of 2-4 nm). Moreover, the thickness of the carbon layer (CL) was found to increase from 1400 to 1700 ℃. The high-resolution image (Figure 12b) illustrates that the carbon phase has an interplanar spacing of 0.34 nm, which is similar to graphitic carbon;[48] however, the TEM micrographs as well as Raman spectroscopy data (shown in Supplementary Information) indicate that the encapsulating carbon phase has a rather highly disordered / turbostratic nature.

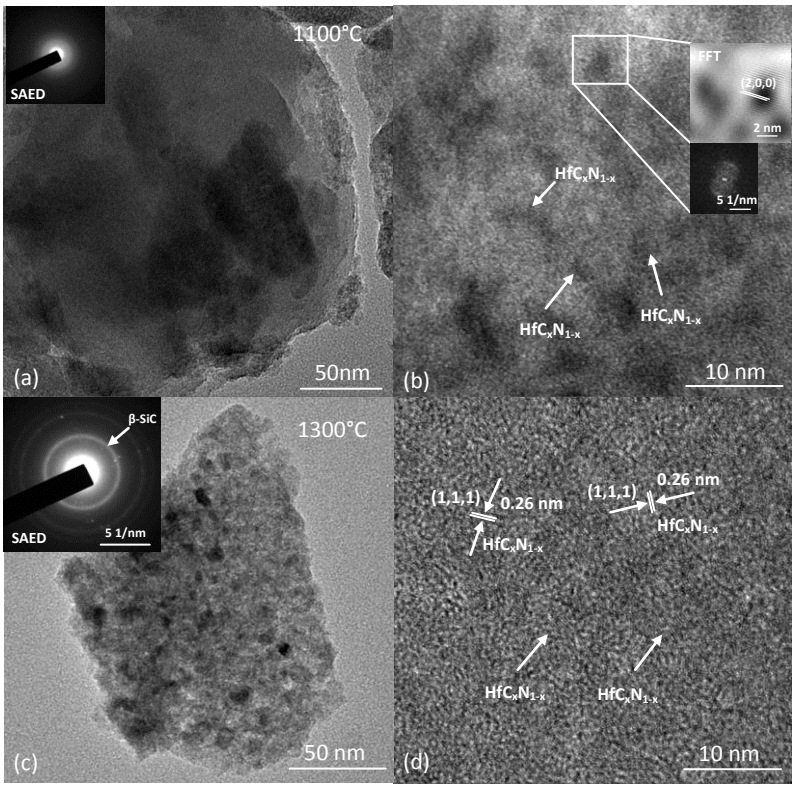

Figure 11. TEM images of SHC-1100 (a and b) and SHC-1300 (c and d).

Based on previous research reports, metal nanoparticles such as Fe encapsulated by carbon layer have been developed. The carbon layer was shown to act a diffusion barrier and thus to prevent the growth of the nanoparticles.[49,50] In the present study, the HfC_xN_{1-x} particles are embedded in a 2-4 nm thick carbon layer (Figures 12b and 12d), which effectively inhibits their coarsening even at very high temperatures. As can be taken from the TEM images, the average particle size of HfC_xN_{1-x} annealed at 1400 ℃ and 1700 ℃ amounts 8 and 37 nm, respectively. Thus, the HfC_xN_{1-x} precipitations do not increase significantly in size upon increasing the annealing the temperature. The average size of both HfC_xN_{1-x} and β-SiC was found to be less than 55 nm even after annealing at 1800 ℃ (Table 3). This type of microstructure has also been reported in B_4C/SiC and SiC/Fe/C ceramic nanocomposites as well as ZrC-containing C/C composites.[27,48,51] However, the mechanism of its formation is not clear yet.

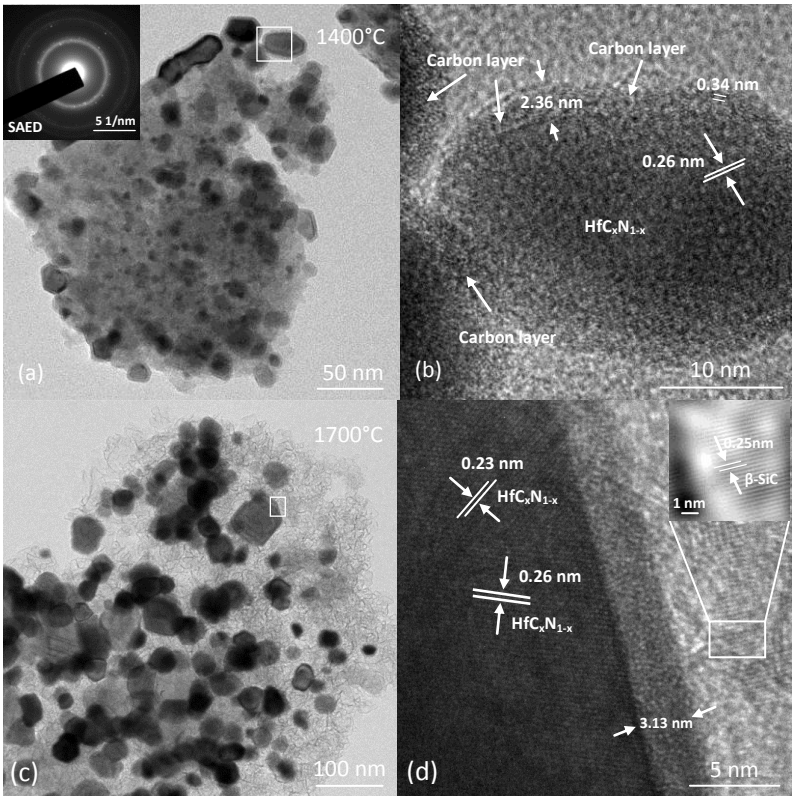

Figure 12. TEM micrographs of SHC-1400 (a and b - b is a high-resolution image magnified from the white rectangular area in a) and SHC-1700 (c and d - d is a high-resolution image magnified from the white rectangular area in c).

The ceramic powder prepared at 1100 ℃ (i.e., SiHC-1100) was used to synthesize dense monolithic SiC/HfC_xN_{1-x}-based nanocomposites using plasma spark sintering (SPS). After sintering at 2200 ℃ (50 MPa, 30 min dwell), dense SiC/HfC_xN_{1-x}-based monoliths with residual porosity of 0.74 vol% and a skeletal density of 3.72 g cm^{-3} were obtained. The XRD pattern of the monolithic sample (Figure 10a) reveals that HfC_xN_{1-x} and β-SiC phases are formed after sintering at 2200 ℃ and the estimated composition of HfC_xN_{1-x} was $HfC_{0.83}N_{0.17}$. The average sizes of β-SiC and HfC_xN_{1-x} nanoparticles were ca. 37 and 81 nm, respectively.

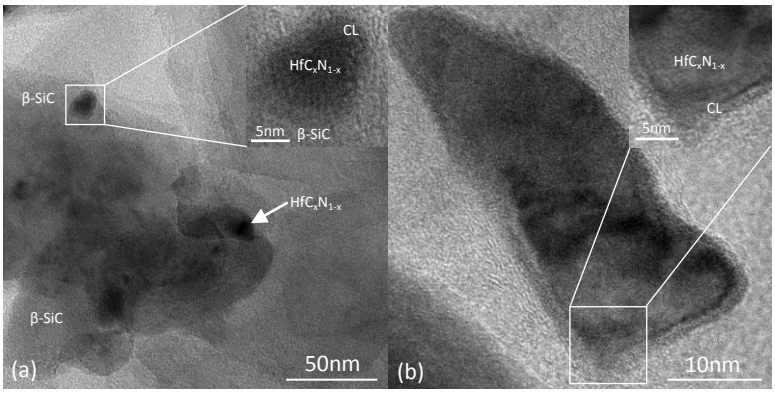

Figure 13. TEM micrographs of monolithic SiC/HfC_xN_{1-x}-based ceramic nanocomposites prepared upon SPS at 2200 ℃ (CL: carbon layer).

Representative TEM micrographs of the monolithic ceramic nanocomposite are shown in Figure 13 and indicate that the HfC_xN_{1-x} particles were encapsulated by a carbon layer, as also observed for the powder samples annealed at high temperatures and thus explaining the nanoscaled microstructure in the obtained monolithic sample.

Electrical conductivity of the synthesized monolithic SiC/HfC_xN_{1-x} nanocomposites

The electrical conductivity was measured 3 times on each side of the dense monolithic SiC/HfC_xN_{1-x} nanocomposite and Hf-free SiC-based ceramics using currents of 10, 30 and 50 mA at 20 ℃. The results showed that the average electrical conductivity of the dense monolithic SiC/ HfC_xN_{1-x} nanocomposite is 136.24 S/cm and the dense monolithic Hf-free SiC ceramic possesses an electrical conductivity of 1.83 S/cm. As reported in the literature, the electrical conductivity of pure β-SiC at ambient temperature is ca. 1.8×10^{-3} S/cm[52] while the polymer derived β-SiC-based ceramics especially the β-SiC fibers have electrical conductivity higher than 1.2 S/cm. This feature is mainly due to the presence of free carbon and to the microstructure and microtexture of the polymer derived SiC ceramics[53]. In the present study, the free carbon has been also shown to highly enhance (ca. three orders

of magnitude) the electrical conductivity of the dense monolithic Hf-free SiC-based ceramic as compared to that of pure β-SiC. Moreover, the dense monolithic SiC/HfC_xN_{1-x}-based nanocomposite which in addition to free carbon contains ca. 8.6 vol% of $HfC_{0.83}N_{0.17}$ (Table 3) exhibits a two order of magnitudes higher electrical conductivity than that of the polymer-derived monolithic Hf-free SiC-based sample (136 vs. 1.8 S/cm). This finding relies on the electrical conductivity of cubic HfN, HfC and their solid solutions (with values in the order of 10^4 S/cm)[4] and on the fact that the $HfC_{0.83}N_{0.17}$ nano-grains are homogeneously distributed within the SiC/HfC_xN_{1-x}-based nanocomposites.

CONCLUSIONS

Dense monolithic SiC/HfC_xN_{1-x}-based nanocomposites can be prepared upon SPS processing of a single-phase amorphous SiHfCN-based ceramic which was synthesized from a single-source precursor. The ceramization of the single-source precursor indicates that the Hf incorporation significantly increases the cross-linking degree of the polymeric backbone and consequently the ceramic yield was as high as 80 wt% upon pyrolysis at *ca*. 900 ℃. The resulting single-phase amorphous SiHfCN was found to undergo phase separation at temperatures beyond 1100 ℃, leading to the formation of amorphous SiC, HfC_xN_{1-x} and segregated carbon. By annealing the amorphous ceramic at temperatures of 1400 to 1800 ℃, a unique microstructure was obtained, consisting of HfC_xN_{1-x} nanoparticles dispersed within a β-SiC matrix and encapsulated by a 2-4 nm thick carbon layer. This microstructural feature is considered to be responsible for the microstructural stability of the ceramic nanocomposites upon exposition to high temperatures, which allows for preparing nano-scaled ultrahigh temperature ceramics. Moreover, a dense monolithic SiC/HfC_xN_{1-x}-based nanocomposite (SiC/$HfC_{0.83}N_{0.17}$) was successfully prepared by SPS using the SiHfCN-based ceramic powder synthesized at 1100 ℃. The grain size of both SiC and $HfC_{0.83}N_{0.17}$ are less than 100 nm. Also the dense monolithic nanocomposite

is characterized by HfC_xN_{1-x} grains encapsulated by an *in situ* formed carbon layer and embedded homogeneously in a β-SiC matrix. The presence of segregated carbon and of well dispersed $HfC_{0.83}N_{0.17}$ nano-particles with metallic character within the microstructure of the prepared SiC/HfC_xN_{1-x}-based nanocomposites has been found to be responsible for a significant increase of the electrical conductivity as compared to monolithic Hf-free and polymer-derived SiC ceramics prepared under similar conditions.

AUTHOR INFORMATION

*Corresponding Author: **Zhaoju Yu** (zhaojuyu@xmu.edu.cn).

ACKNOWLEDGEMENT

Zhaoju Yu thanks the National Natural Science Foundation of China (No. 50802079) and Scientific and Technological Innovation Platform of Fujian Province (2006L2003) for financial support. Qingbo Wen acknowledges the China Scholarship Council (CSC) for financial support (No. 201206130059).

Supplementary Information (SI) Available: Raman spectroscopy characterization of the SiHfCN-based ceramics is available.

REFERENCES

1. W. G. Fahrenholtz, G. E. Hilmas, I. G. Talmy and J. A. Zaykoski, *Journal of the American Ceramic Society*, 2007, **90**, 1347-1364.
2. R. Savino, M. De Stefano Fumo, D. Paterna, A. Di Maso and F. Monteverde, *Aerospace Science and Technology*, 2010, **14**, 178-187.
3. E. Wuchina, E. Opila, M. Opeka, W. Fahrenholtz and I. Talmy, *The Electrochemical Society Interface*, 2007, **16**, 30.
4. H. O. Pierson, *Handbook of Refractory Carbides & Nitrides: Properties, Characteristics,*

Processing and Apps, William Andrew, 1996.

5. L. Silvestroni, D. Sciti, J. Kling, S. Lauterbach and H. J. Kleebe, *Journal of the American Ceramic Society*, 2009, **92**, 1574-1579.
6. R. Savino, M. De Stefano Fumo, L. Silvestroni and D. Sciti, *Journal of the European Ceramic Society*, 2008, **28**, 1899-1907.
7. R. W. Rice, C. C. Wu and F. Boichelt, *Journal of the American ceramic society*, 1994, **77**, 2539-2553.
8. F. Knudsen, *Journal of the American Ceramic Society*, 1959, **42**, 376-387.
9. M. M. Opeka, I. G. Talmy, E. J. Wuchina, J. A. Zaykoski and S. J. Causey, *Journal of the European Ceramic Society*, 1999, **19**, 2405-2414.
10. W. A. Sanders and S. J. Grisaffe, *THE HOT-PRESSING OF HAFNIUM CARBIDE (MELTING POINT, 6030 F)*, National Aeronautics and Space Administration. Lewis Research Center, Cleveland, 1960.
11. S.-K. Sun, G.-J. Zhang, W.-W. Wu, J.-X. Liu, T. Suzuki and Y. Sakka, *Scripta Materialia*, 2013, **69**, 139-142.
12. D. Sciti, S. Guicciardi and M. Nygren, *Journal of the American Ceramic Society*, 2008, **91**, 1433-1440.
13. S. Shimada, M. Inagaki and K. Matsui, *Journal of the American Ceramic Society*, 1992, **75**, 2671-2678.
14. P. Sarin, P. Driemeyer, R. Haggerty, D.-K. Kim, J. Bell, Z. Apostolov and W. Kriven, *Journal of the European Ceramic Society*, 2010, **30**, 2375-2386.
15. H. Jiecai, H. Ping and Z. Xinghong, *Composites Science and Technology*, 2008, **68**, 799-806.
16. F. Monteverde and L. Scatteia, *Journal of the American Ceramic Society*, 2007, **90**, 1130-1138.
17. J. W. Zimmermann, G. E. Hilmas and W. G. Fahrenholtz, *Materials Chemistry and Physics*, 2008, **112**, 140-145.
18. H. Gleiter, *Nanostructured materials*, 1995, **6**, 3-14.
19. K. Niihara, *Nippon seramikkusu kyokai gakujutsu ronbunshi*, 1991, **99**, 974-982.
20. A. Sawaguchi, K. Toda and K. Niihara, *Journal of the American Ceramic Society*, 1991, **74**, 1142-1144.
21. E. Ionescu, H.-J. Kleebe and R. Riedel, *Chemical Society Reviews*, 2012, **41**, 5032-5052.
22. E. Ionescu, C. Linck, C. Fasel, M. Müller, H. J. Kleebe and R. Riedel, *Journal of the American Ceramic Society*, 2010, **93**, 241-250.
23. E. Ionescu, B. Papendorf, H. J. Kleebe, F. Poli, K. Müller and R. Riedel, *Journal of the American Ceramic Society*, 2010, **93**, 1774-1782.
24. M. Huang, Y. Fang, R. Li, T. Huang, Z. Yu and H. Xia, *Journal of applied polymer science*, 2009, **113**, 1611-1618.
25. N. Klymko, *Future Fab International Issue-Metrology Analysis*, 2004, **8**, 17.
26. K. Li, S. Li, N. Li, D. A. Dixon and T. M. Klein, *The Journal of Physical Chemistry C*, 2010, **114**, 14061-14075.
27. Z. Yu, L. Yang, H. Min, P. Zhang, C. Zhou and R. Riedel, *Journal of Materials Chemistry C*, 2014, **2**, 1057-1067.
28. E. Ionescu, B. Papendorf, H.-J. Kleebe, H. Breitzke, K. Nonnenmacher, G. Buntkowsky and R. Riedel, *Journal of the European Ceramic Society*, 2012, **32**, 1873-1881.
29. H. G. Woo and T. D. Tilley, *Journal of the American Chemical Society*, 1989, **111**, 8043-8044.

30. K. Brandstadt, S. Cook, B. T. Nguyen, A. Surgenor, R. Taylor and M. S. Tzou, Google Patents, 2013.
31. Q. D. Nghiem, A. Asthana, I.-K. Sung and D.-P. Kim, *Journal of materials research*, 2006, **21**, 1543-1549.
32. I. Rushkin, Q. Shen, S. Lehman and L. Interrante, *Macromolecules*, 1997, **30**, 3141-3146.
33. J. Schuhmacher, F. Berger, M. Weinmann, J. Bill, F. Aldinger and K. Müller, *Applied organometallic chemistry*, 2001, **15**, 809-819.
34. C. Gérardin, F. Taulelle and D. Bahloul, *Journal of Materials Chemistry*, 1997, **7**, 117-126.
35. E. Ionescu, B. Papendorf, H. J. Kleebe and R. Riedel, *Journal of the American Ceramic Society*, 2010, **93**, 1783-1789.
36. S. Widgeon, S. Sen, G. Mera, E. Ionescu, R. Riedel and A. Navrotsky, *Chemistry of Materials*, 2010, **22**, 6221-6228.
37. S. Dirè, R. Ceccato, S. Gialanella and F. Babonneau, *Journal of the European Ceramic Society*, 1999, **19**, 2849-2858.
38. G. T. Burns, R. B. Taylor, Y. Xu, A. Zangvil and G. A. Zank, *Chemistry of materials*, 1992, **4**, 1313-1323.
39. S. Kaur, R. Riedel and E. Ionescu, *Journal of the European Ceramic Society*, 2014, doi: 10.1016/j.jeurceramsoc.2014.1005.1002.
40. H. J. Kleebe, K. Nonnenmacher, E. Ionescu and R. Riedel, *Journal of the American Ceramic Society*, 2012, **95**, 2290-2297.
41. K. Nonnenmacher, H. J. Kleebe, J. Rohrer, E. Ionescu and R. Riedel, *Journal of the American Ceramic Society*, 2013, **96**, 2058-2060.
42. S. Widgeon, G. Mera, Y. Gao, E. Stoyanov, S. Sen, A. Navrotsky and R. Riedel, *Chemistry of Materials*, 2012, **24**, 1181-1191.
43. S. Widgeon, G. Mera, Y. Gao, S. Sen, A. Navrotsky and R. Riedel, *Journal of the American Ceramic Society*, 2013, **96**, 1651-1659.
44. U. Mizutani, *Hume-Rothery rules for structurally complex alloy phases*, CRC Press, 2010.
45. J. M. Córdoba, M. J. Sayagués, M. D. Alcalá and F. Gotor, *Journal of the American Ceramic Society*, 2007, **90**, 381-387.
46. K. Aigner, W. Lengauer, D. Rafaja and P. Ettmayer, *Journal of alloys and compounds*, 1994, **215**, 121-126.
47. J. M. Cordoba, M. J. Sayagués, M. D. Alcala and F. J. Gotor, *Journal of the American Ceramic Society*, 2005, **88**, 1760-1764.
48. M. M. Guron, X. Wei, D. Welna, N. Krogman, M. J. Kim, H. Allcock and L. G. Sneddon, *Chemistry of Materials*, 2009, **21**, 1708-1715.
49. Y. Lu, Z. Zhu and Z. Liu, *Carbon*, 2005, **43**, 369-374.
50. J. Gim, V. Mathew, J. Lim, J. Song, S. Baek, J. Kang, D. Ahn, S.-J. Song, H. Yoon and J. Kim, *Scientific reports*, 2012, **2**.
51. Z. Chen, W. Wu, Z. Chen, X. Cong and J. Qiu, *Ceramics International*, 2012, **38**, 761-767.
52. B. Zhang, J. Li, J. Sun, S. Zhang, H. Zhai and Z. Du, *Journal of the European Ceramic Society*, 2002, **22**, 93-99.
53. G. Chollon, R. Pailler, R. Canet and P. Delhaes, *Journal of the European Ceramic Society*, 1998, **18**, 725-733.